



## Supporting Information

for *Small*, DOI: 10.1002/smll.201802891

### Biophysical Phenotyping and Modulation of ALDH+ Inflammatory Breast Cancer Stem-Like Cells

*Weiqiang Chen,\* Steven G. Allen, Weiyi Qian, Zifeng Peng,  
Shuo Han, Xiang Li, Yubing Sun, Chelsea Fournier, Liwei  
Bao, Raymond H. W. Lam, Sofia D. Merajver,\* and Jianping  
Fu\**

## Supporting Information

### Biophysical Phenotyping and Modulation of ALDH<sup>+</sup> Inflammatory Breast Cancer Stem-like Cells

Weiqliang Chen<sup>#</sup>, Steven G. Allen<sup>#</sup>, Weiyi Qian, Zifeng Peng, Shuo Han, Xiang Li, Yubing Sun, Chelsea Fournier, Liwei Bao, Raymond H.W. Lam, Sofia D. Merajver<sup>\*</sup>, and Jianping Fu<sup>\*</sup>

<sup>#</sup>Contributed equally to this work; <sup>\*</sup>Correspondence and requests for materials should be addressed to W.C. (wchen@nyu.edu), J.F. (jpfu@umich.edu) or S.D.M. (smerajve@umich.edu).

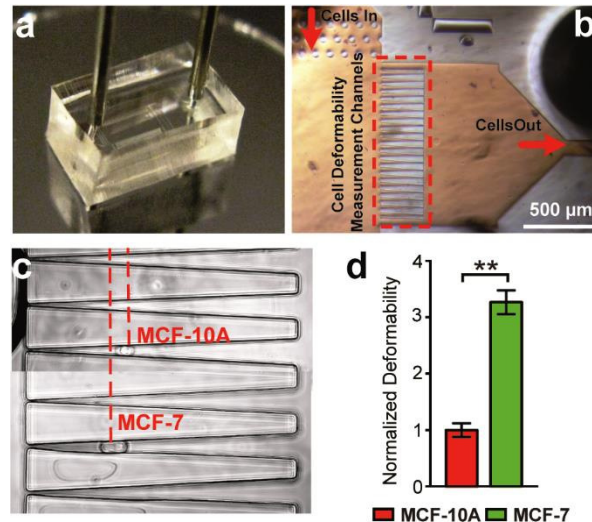


**Figure S1. Microfluidic deformability microcytometer device for single cell deformability measurements.** (a) Photo showing the microfluidic deformability microcytometer for single cell deformability measurements. (b) Brightfield image showing structure of the deformability microcytometer. (c) Representative brightfield images showing breast cells (MCF-10A) and breast cancer cells (MCF-7) trapped in the deformability microcytometer under differential pressure across the tapped channels. (d) Normalized cell deformability of MCF-10A and MCF-7 cells. Error bars represent  $\pm$  s.e.m. ( $n > 20$ ).  $p$ -value was calculated using the student  $t$ -test. \*\* ( $p < 0.01$ ).

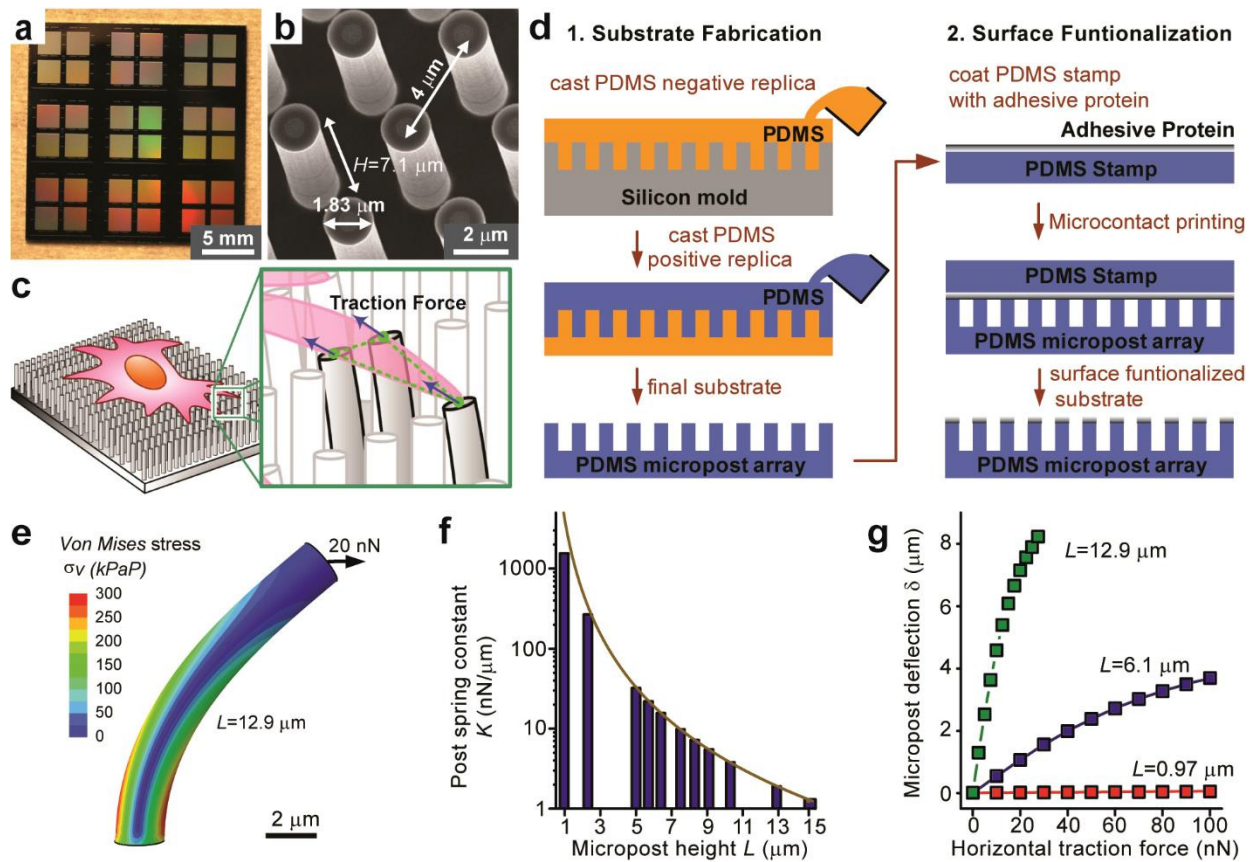


**Figure S2. Fabrication and characterization of PDMS micropost arrays.** (a) Representative photograph of the silicon micropost array master. (b) SEM image of microfabricated hexagonally arranged silicon micropost array master with post geometrical factors indicated. (c) Schematic of using PDMS microposts as force sensors for subcellular traction force measurements. (d) Fabrication of PDMS micropost arrays involves standard photolithography and deep reactive-ion etching (DRIE) for the silicon micropost array master in a cleanroom environment, and then replica molding with PDMS to generate the final PDMS micropost array. (e) Finite-element method (FEM) analysis of micropost bending in response to a horizontal traction force  $F$  of 20 nN. Values of Von Mises stress,  $\sigma_v$ , are plotted ( $\sigma_v = 0.707 \cdot [(\sigma_1 - \sigma_2)^2 + (\sigma_2 - \sigma_3)^2 + (\sigma_1 - \sigma_3)^2]^{1/2}$ , where  $\sigma_1$ ,  $\sigma_2$ , and  $\sigma_3$  are the principle stresses in orthogonal directions). (f) Dependence of nominal spring constant  $K$  of PDMS micropost on micropost height  $L$ , as computed from FEM (bars), and from the Euler-Bernoulli beam theory (dark yellow curve).  $K$  is determined as  $K = dF / d\delta$  ( $\delta \rightarrow 0$ ). (g) Micropost deflection  $\delta$  as a function of  $F$  for PDMS microposts of different heights, as calculated by FEM analysis ( $L = 0.97 \mu\text{m}$  (red),  $L = 6.1 \mu\text{m}$  (blue), and  $L = 12.9 \mu\text{m}$  (green)).

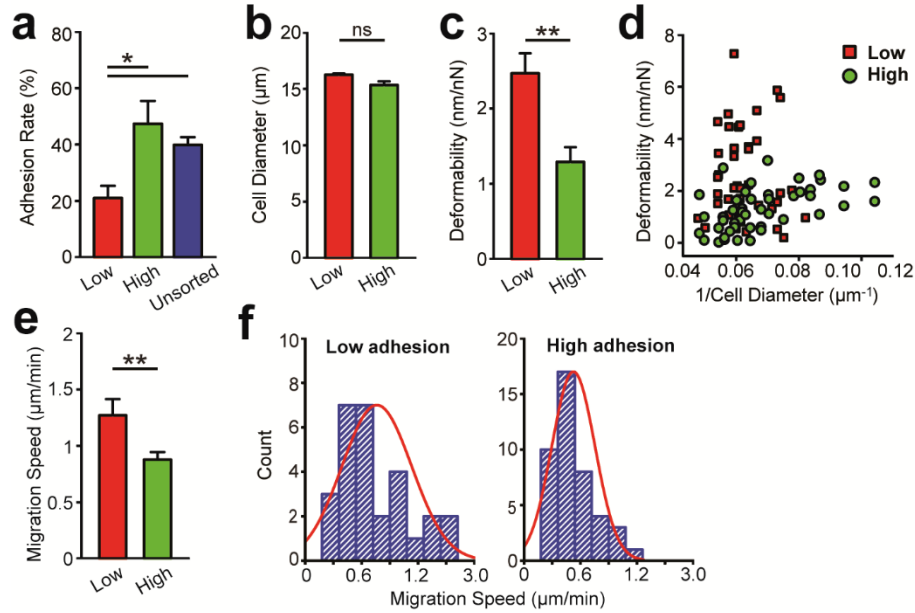


**Figure S3. Functional and biophysical characterization of SUM149 cells selected by cell adhesion strength.** (a) Quantified adhesion rate of selected low-adhesion, high-adhesion and unsorted SUM149 cells. (b) Quantified cell diameter of selected low-adhesion and high-adhesion SUM149 cells. (c) Cell deformability of isolated low-adhesion and high-adhesion SUM149 IBC cells. (d) Cell deformability plotted as a function of cell diameter. Each data point represents an individual cell. (e) Average and (f) distribution of migration speed for single selected low-adhesion and high-adhesion SUM149 cells measured by the Cellomics Cell Motility kit. Error bars represent  $\pm$  s.e.m. ( $n > 20$ ).  $p$ -value was calculated using the student t-test. ns ( $p > 0.05$ ) and \*\* ( $p < 0.01$ ).

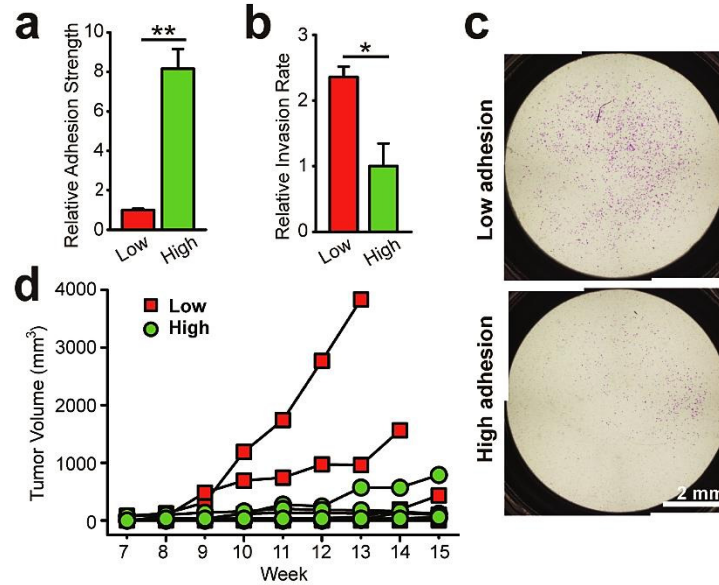


**Figure S4. Adhesion-based selection of CSC-like SUM159 IBC cells with higher tumorigenic ability.** (a) Quantified adhesion strengths of isolated low-adhesion and high-adhesion SUM159 cells. (b) Relative invasion rate and (c) representative images from in vitro invasion assays performed for isolated low-adhesion and high-adhesion SUM159 cells using the Biocoat Matrigel Invasion Chambers. In c, invading cells were fixed with formaldehyde before stained with 1% crystal violet. (d) Tumor volumes over time in xenograft mice (total 5 mice for each group) using isolated low-adhesion and high-adhesion SUM159 cells. For a&b, error bars represent  $\pm$  s.e.m. p-values were calculated using the student t-test; \* ( $p < 0.05$ ), \*\* ( $p < 0.01$ ).

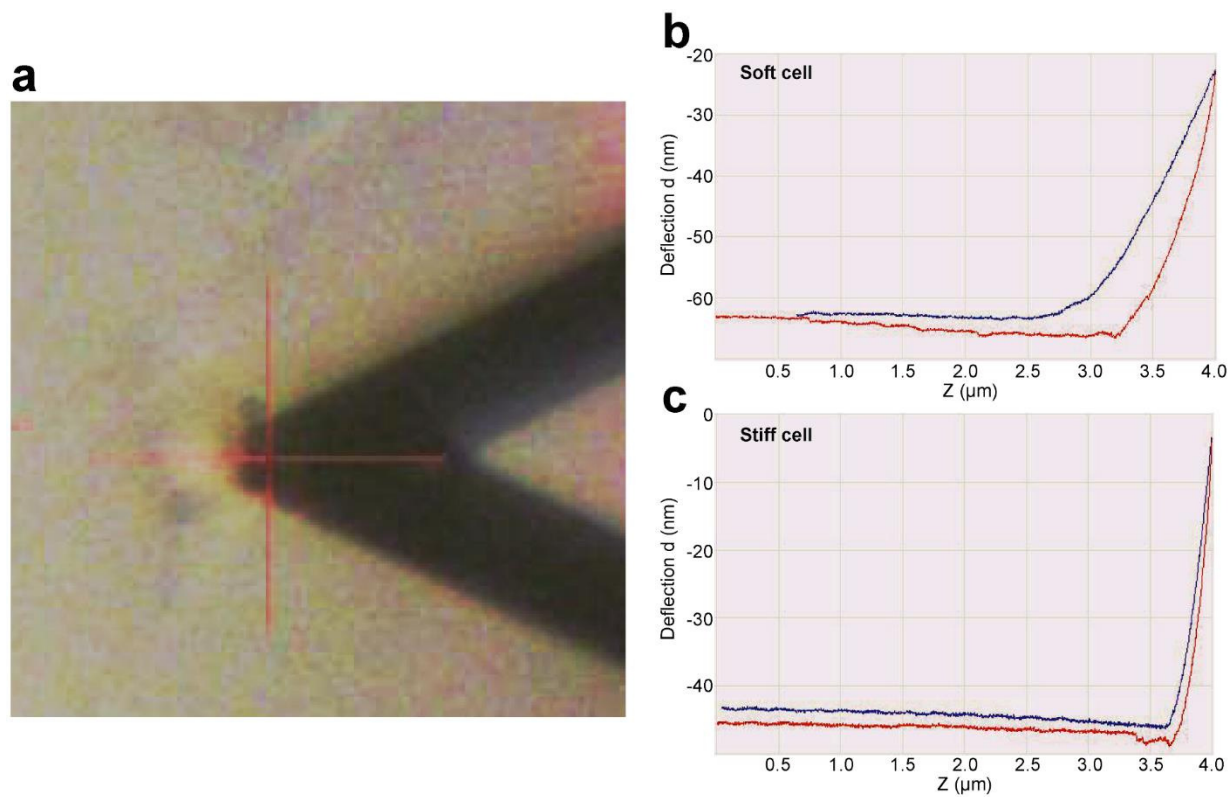


**Figure S5. AFM measurement of cell stiffness.** (a) Representative image showing an AFM tip on a single SUM149 cell on stiff PMA captured by the optical microscopy during AFM measurement. (b&c) Cantilever deflection versus the piezo movement (with the reference corresponds to the highest location of the scanner) on a soft (b) and a stiff (c) cell.